Lack of mutant huntingtin in cortical efferents improves behavioral inflexibility and corticostriatal dynamics in Huntington's disease mice

Ana María Estrada-Sánchez[1,2,*], Courtney L. Blake[1], Scott J. Barton[1], Andrew G. Howe[3,4] and George V. Rebec[1,*]

1 Program in Neuroscience and Department of Psychological and Brain Sciences, Indiana University, Bloomington, Indiana 47405.

2 Departmento de Biología Molecular. Instituto Potosino De Investigación Científica y Tecnológica, Camino a la Presa San José 2055, Col. Lomas 4ª Sección, CP 78216, San Luis Potosí, México

3 Neuroscience Interdepartmental Program, University of California Los Angeles, Los Angeles, CA, 90095, USA.

4 Psychology Department, University of California Los Angeles, Los Angeles, California 90045.

AMES, GVR conceived and designed the experiments. AMES and CLB performed the experiments. AMES, CLB, AGH and SJB analyzed the data. AMES and GVR wrote the paper with inputs from CLB, AGH and SJB.

Running head: Role of cortical outputs in Huntington's disease motor inflexibility

*** Corresponding author:**

- George V. Rebec, Ph.D.; Department of Psychological and Brain Sciences, and Program in Neuroscience, 1101 E. 10th St., Bloomington, IN 47405; tel: (812) 855-4832 office; fax: (812) 855-4520; E-mail: rebec@indiana.edu

Keywords: BACHD, cortical outputs, motor inflexibility, local field potentials, plus-shaped maze, M1, dorsal striatum.

Glossary

BACHD: bacterial artificial chromosome Huntington's disease model

BE: BACHD/Emx1-Cre, conditional model

DS: Dorsal striatum

HD: Huntington's disease

HTT: huntingtin gene

mHTT: mutant huntingtin gene

LFPs: local field potentials

M1: cortical motor area 1

R6/2: truncated transgenic mouse model of Huntington's disease

WT: wild-type

Abstract

Abnormal communication between cerebral cortex and striatum plays a major role in the motor symptoms of Huntington's disease (HD), a neurodegenerative disorder caused by a mutation of the huntingtin gene (mHTT). Because cortex is the main driver of striatal processing, we recorded local field potential (LFP) activity simultaneously in primary motor cortex (M1) and dorsal striatum (DS) in BACHD mice, a full-length HD gene model, and in a conditional BACHD/Emx-1 Cre (BE) model in which mHTT is suppressed in cortical efferents, while mice freely explored a plus-shaped maze beginning at 20 weeks of age. Relative to wild-type (WT) controls, BACHD mice were just as active across >40 weeks of testing but became progressively less likely to turn into a perpendicular arm as they approached the choice point of the maze, a sign of HD motor inflexibility. BE mice, in contrast, turned as freely as WT throughout testing. Although BE mice did not exactly match WT in LFP activity, the reduction in alpha (8-13 Hz), beta (13-30 Hz), and low gamma (30-50 Hz) power that occurred in M1 of turning-impaired BACHD mice was reversed. No reversal occurred in DS. In fact, BE mice showed further reductions in DS theta (4-8 Hz), beta, and low gamma relative to the BACHD model. Coherence analysis indicated a dysregulation of corticostriatal information flow in both BACHD and BE mice. Collectively, our results suggest that mHTT in cortical outputs drives the dysregulation of select cortical frequencies that accompany the loss of behavioral flexibility in HD.

New & Noteworthy

BACHD mice – a full-length genetic model of Huntington's disease (HD) – express aberrant local field potential (LFP) activity in primary motor cortex (M1) along with decreased probability of turning into a perpendicular arm of a plus-shaped maze, a motor inflexibility phenotype. Suppression of the mutant huntingtin gene in cortical output neurons prevents decline in turning and improves alpha, beta, and low gamma activity in M1. Our results implicate cortical networks in the search for therapeutic strategies to alleviate HD motor signs.

Introduction

Huntington's disease (HD) is an autosomal dominant neurodegenerative disorder caused by an increased number of CAG repeats in the huntingtin (HTT) gene (Gusella et al. 1983; The Huntington's Disease Collaborative Research Group 1993). Although the behavioral phenotype includes psychiatric and cognitive disturbances, the onset of motor abnormalities, including impaired coordination and involuntary generalized movements, is a defining feature. At a neuropathological level, early signs of HD occur in conjunction with dysfunctional activity in the corticostriatal network followed by the eventual loss of cortical pyramidal neurons and the medium spiny neurons they target in dorsal striatum (DS) (De la Monte et al. 1988). Neuroimaging studies of HD patients indicate a direct relationship between the thinning of motor cortical areas and motor abnormalities (Rosas et al. 2008). In fact, postmortem analysis reveals that the extent of loss of neurons in motor cortex of HD patients correlates with the extent of their motor symptoms (Halliday et al. 1998; Thu et al. 2010; Kim et al. 2014). Neuronal loss in other cortical regions is an indicator of mood alterations and cognitive deficits (Halliday et al. 1998; Thu et al. 2010). Together, these studies suggest that cortical neuropathology plays an important role in the development of the HD behavioral phenotype.

Consistent with this view, the conditional BACHD/Emx1-Cre (BE) mouse model, in which mutant HTT (mHTT) is suppressed in cortical output neurons, shows improved corticostriatal synaptic efficacy and reversal of behavioral deficits compared to the full-length BACHD model (Wang et al. 2014). In fact, the behavior-related firing patterns of striatal medium spiny neurons are comparable in BE mice and wild-type (WT) controls but not the full-length BACHD model (Estrada-Sánchez et al. 2015b). Thus, expression of the mutant huntingtin protein in cortical output neurons plays a critical role in shaping aberrant striatal neuronal processing. Here, we used

BE mice to determine if mHTT in cortical efferents is a critical driver of motor inflexibility, an early motor sign of HD defined as a failure to adapt ongoing movement to changes in environmental stimuli (for review see Estrada-Sánchez et al. 2015a). In BACHD and other transgenic mouse models of HD, behavioral inflexibility appears as a decreased probability of turning into a perpendicular arm when mice reach the choice point in a four-arm, plus-shaped maze (Rebec et al. 2003; Estrada-Sánchez et al. 2013a; Hong et al. 2012a). We recorded local field potential (LFP) activity simultaneously in primary motor cortex (M1) and DS immediately before and after choice-point entry in BACHD, BE, and WT mice. Recordings occurred at regular intervals beginning at 20 weeks of age and continuing for >40 weeks thereafter, sufficient time for turning probability to decline in the BACHD model. We analyzed power spectral density as well as corticostriatal coherence to determine the impact of cortical mHTT suppression in the onset and progression of turning-related deficits.

Methods

Animal care and housing

Animal use was in accord with the National Institutes of Health Guide for the Care and Use of Laboratory Animals and approved by the local Institutional Animal Care and Use Committee. All efforts were made to minimize suffering and the number of animals used in these experiments. Mice, bred from heterozygous pairs (FvB/N background) obtained from X. W. Yang at the University of California, Los Angeles, were housed in the Psychology building at Indiana University, Bloomington under controlled temperature and humidity conditions. Mice were maintained on a 12-h light/dark cycle with free access to food and water.

Because motor changes observed in BACHD mice worsen progressively with age and independently of gender (Gray et al. 2008), data were obtained from assorted male and female WT (n=6; 3 female and 3 males), BE (n=6; 3 female and 3 males) and BACHD (n=6; 4 female and 2 males) mice. The BACHD model expresses full-length human mHTT containing 97 glutamine repeats. BE mice are a conditional model produced by crossing BACHD mice with Emx1-Cre mice. Emx1-Cre mice express the Cre recombinase enzyme in forebrain glutamate-projection neurons. Crossing BACHD/Emx1-Cre generates the conditional BE mouse model in which mHTT is suppressed only in cortical output neurons (Wang et al. 2014; Estrada-Sánchez et al. 2015b).

Genotyping

Genotyping was carried out as previously described (Estrada-Sánchez et al. 2015b). In brief, DNA extract was diluted with 350 µL filter-sterilized water, heated to 100°C for 10 min, centrifuged for 2 min at 17,000 X g, and stored at 4°C. The forward and reverse primers for the CAG repeat region in mHTT were 5'-ATG AAG GCC TTC GAG TCC CTC AAG TCC TTC-3' and 5'-GGC GGC TGA GGA AGC TGA GGA-3', respectively. The forward and reverse primers for the Cre marker were 5'-GCG TTC CCC AGA GCC CCG CTA CCT C-3' and 5'-GGA TCC GCC GCA TAA CCA GTG-3', respectively. PCR-cycling conditions for both mHTT and the Cre marker with MyTaq™ Red Mix were 94°C for 180 s followed by 30 cycles of 94°C for 30 s, 60°C for 20 s, and 72°C for 30 s, with a final elongation at 72°C for 10 min. Sample electrophoresis was performed in type I agarose with 0.2 µg/mL ethidium bromide at 5 V/cm for 180 min using a 100-base pair ladder as DNA standard. Gels were evaluated with Kodak Image Station 4000R and Kodak Molecular Imaging software (Carestream Molecular Imaging, New Haven, CT) to confirm genotype.

Electrodes and implantation surgery

Electrode bundles were built in-house; each consisted of four recording electrodes (25 μm diameter insulated stainless steel micro-wires) and 2 (50 μm diameter uninsulated stainless-steel ground wires; California Fine Wire, Grover Beach, CA). Each wire was friction-fitted to gold-plated pin connectors into polyphenylene sulfide insulators (7x6x4 mm) (Omnetics Connector Corporation, Minneapolis, MN, USA). Two sets of these insulators were glued together to obtain two electrode bundles. To record M1 and DS activity simultaneously, one micro-wire bundle was cut to 0.5 mm in length, while the second was cut to 3.0 mm. The electrode assembly was small, lightweight, and well tolerated by the mice to allow free movement (Hong et al. 2012a).

For electrode implantation, mice received meloxicam (1 mg/kg, subcutaneously) followed by anesthesia with a mixture of chloral hydrate and sodium pentobarbital (chloropent: 170 mg/kg chloral hydrate and 40 mg/kg sodium pentobarbital) administered intraperitoneally at 0.4 mL/100g body weight (WT = 31.7 ± 1.8; BE = 31.4 ± 1.8; BACHD = 38.5 ± 3.3; No differences between groups was observed $F(2, 15) = 2.61$. $P = 0.105$). Mice were mounted in a stereotaxic frame, and following a midline scalp incision, a hole was drilled +0.5 mm anterior and ±1.5 mm lateral to Bregma (Paxinos and Franklin 2001). Two additional holes were drilled in the contralateral hemisphere for placement of stainless-steel anchor screws. The multiwire electrode bundles were lowered into M1 and DS (0.5 mm and 3.0 mm ventral to brain surface, respectively). Dental acrylic fixed the electrode assembly in place on the skull. Mice were allowed one week of recovery before testing, which began when mice were ~25 weeks of age, and continued at regular intervals for up to the next ~40 weeks.

Behavioral electrophysiology

LFP activity was recorded during the light phase of the diurnal cycle while the mice freely explored the arms of the plus-shaped maze (see below). Male gold pins attached to a lightweight

flexible wire harness equipped with field-effect transistors were inserted into the head-mounted electrode assembly. The harness was attached to a swivel to allow free movement. LFPs were routed through preamplifiers with 1,000x gain and 0.7-170 Hz filters (Plexon, Dallas, TX, USA).

For each recording session, mice were placed in one arm of the maze and allowed to explore the maze freely for 30 min. Recordings began at 25 weeks of age and continued at roughly bi-weekly intervals for ~40 weeks. Typically, mice move to the center of the maze or choice point, where they have the option to continue straight to the opposite arm or turn 90° to enter either the right or left arm (Rebec et al. 2003). The plus-maze, housed within a sound-attenuating and electrically shielded chamber, is made of Plexiglas® (each arm is 25 cm long and 5 cm wide) and enclosed with 30 cm high Plexiglas® walls (Hong et al. 2012a). The maze is suspended 2 mm above a force-plate actometer (Fowler et al. 2009), which tracks the position of the mouse and the number of turns into each arm. Time-stamps associated with each entry into and exit from the choice point are embedded in the electrophysiological signal. The probability of turning was determined by the sum of arm choices to the right and left arm divided by the total number of choices (left, right, front, and back). The lack of turning behavior is a measure of motor inflexibility, a sign of motor impairment consistently described in HD models (Rebec et al. 2003; Hong et al. 2012a; Estrada-Sánchez et al. 2013a).

Histology

Electrode placement was verified after completion of the final recording session by deeply anesthetizing the mouse with chloropent and running a current pulse (30 μA for 10 s) through each active microwire to mark recording sites. Mice were transcardially perfused with 0.9% saline solution followed by 10% paraformaldehyde. The brain was immediately removed and placed in solution containing 10% potassium ferrocyanide [K4Fe(CN)6] in 10% paraformaldehyde to

produce small blue deposits at the site of the recording. A consecutive series of 40 μm coronal sections of M1 and DS was obtained. Only recordings with confirmed electrode placements were included for analysis.

Statistical analysis

LFP data obtained from each recording session included a time-stamp indicating each entry into the choice point of the plus-shaped maze. LFP activity around the choice point (1 s before and 1 s after entry) was analyzed with NeuroExplorer (Littleton, MA, USA) and MATLAB (Mathworks, Natick, MA, USA) scripts, as previously described by (Hong et al. 2012b). In brief, a Fast Fourier Transform was generated across 0 to 50 Hz frequency range of each signal recorded in M1 and DS (Hong et al. 2012b). Frequency bands are defined as: delta (0.1-4 Hz), theta (4-8 Hz), alpha (8-13 Hz), beta (13-30 Hz) and low gamma (30-50 Hz). Percentage of total power spectral density was calculated in NeuroExplorer and the mean power of each frequency band was calculated for M1 and DS. Coherence analysis also was performed. Coherence values indicate the extent of synchrony between M1 and DS; values range from 0 to 1, where 1 is perfect synchrony between the signals. Relative phase indicates the degree to which M1 and DS signals are in phase (Hong et al. 2012b). Positive, relative-phase values indicate that cortical phase leads, while negative values indicate that DS phase leads (Hong et al. 2012b; Rangel-Barajas et al. 2017). GraphPad Prism version 7 (GraphPad Software, La Jolla, California, USA) was used for statistical analysis of behavioral and LFP data. Percentage of total power spectral density, coherence value, and coherence phase were analyzed by two-way ANOVA followed by Tukey's multiple comparison test.

Behavioral data were collected simultaneously with LFP recordings, but some mice were withdrawn early because the recording system became inoperable (e.g., loss of the headstage). To

account for the missing data points, a mixed-effects model ANOVA with repeated measures was used to determine the effect of age on turning probability and arm entries. Tukey's multiple-comparisons test was used to analyze between-group differences. To include as many mice as possible, we focused on turning probability and arm entries from 25 to 50 weeks of age. In some mice, however, data collection remained robust for several more weeks. To include all animals in a complete picture of maze performance with age, we also used linear regression plots up to 64 weeks of age. Each point in the analysis corresponded to the average (mean) value obtained across mice recorded for each genotype on each test day. For all analyses, differences were considered significant when $p \leq 0.05$.

Results

Turning behavior

Mice were allowed to explore the plus-shaped maze for 30 min during each session. Figure 1A shows the changes in turning probability between 25 and 50 weeks of age. Although WT and BE mice showed an almost identical level of performance, BACHD mice exhibited a significant reduction in turning probability with age that was statistically different from both WT ($p=0.0149$) and BE ($p=0.0343$) mice. As shown in Figure 1B, however, the total number of arm entries was not statistically different (n=50 trials for WT; n=56 trials for BACHD; n=60 trials for BE mice), indicating that the decline in turning probability in aging BACHD mice cannot be explained by an overall decrease in movement throughout the maze.

Our linear regression analysis on mice that remained available for testing out to 64 weeks of age confirms a BACHD decline in turning probability, as evidenced by a significant deviation from zero slope (Figure 1C; $p=0.0006$, $r^2= 0.15$, n=76 sessions). WT and BE mice show no such deviation ($p=0.363$, $r^2=0.013$, n=67 sessions for WT; and $p=0.108$, $r^2=0.034$, n=73 sessions for

BE). The slope for arm entry is not significantly different from zero for all groups (Figure 1D; $p=0.10$, $r^2=0.041$, $n=67$ for WT; $p=0.80$, $r^2=0.00085$, $n=73$ for BE; and $p=0.28$, $r^2=0.015$, $n=76$ for BACHD).

Overall, our results indicate that BACHD mice develop an aging-related decline in turning probability, a sign of motor inflexibility, which did not occur in the BE model. Importantly, the decline in BACHD turning probability is not due to a lack of exploration of the maze arms.

LFP activity

As BACHD mice exhibit a progressive decline in turning behavior with age, we evaluated corresponding LFP activity in the oldest mice (from 50 to 64 weeks of age). As shown schematically in Figure 2, histological analysis confirmed all electrode placements in M1 and DS.

The percentage of total power spectral densities (where the sum of all power spectrum values equal 100) was calculated for all mice tested between 50 and 64 weeks of age as they entered and exited the choice point of the maze (1 s before and after choice-point entry). In this age range, when turning deficits were readily apparent in BACHD mice, corresponding M1 activity was characterized by significant decreases in theta ($p<0.0001$), alpha ($p<0.0001$), beta ($p<0.0001$) and low gamma activity ($p<0.0001$) relative to WT, as shown in Figure 3A-E. A slight difference in delta frequency was observed between groups, but was only statistically different between WT and BACHD mice ($p=0.0471$). BE mice were intermediate, showing a significant improvement over BACHD in alpha ($p<0.0001$), beta ($p<0.0001$), and low gamma ($p<0.0001$) power, but significantly below WT ($p<0.0001$) for all three frequency bands as well as theta ($p=0.0004$).

LFP changes also occurred in DS. As shown in Figure 4A-E, while no difference was observed in delta frequency, BACHD mice responded with a significant decrease in theta ($p=0.003$), alpha ($p<0.0001$), beta ($p<0.0001$), and low gamma ($p<0.0001$). In contrast with the

changes observed in M1, BE mice showed a further reduction in theta ($p=0.0017$), beta ($p=0.0024$) and low gamma ($p=0.0008$) relative to BACHD, while BE and BACHD alpha power were not significantly different ($p=0.284$).

Functional relationship between M1 and DS LFPs

Coherence analysis was performed in a further assessment of the functional relationship between M1 and DS signaling. Figure 5 shows the coherence value across all examined frequencies. Note that coherence value decreases as frequency increases. When comparing coherence values grouped by frequency band and analyzed across genotypes, we observed that relative to WT, both BACHD ($p<0.0001$ for all frequencies) and BE ($p<0.0001$ for all frequencies) mice showed an increase in delta, theta, alpha, beta, and low gamma coherence (Figure 5). Interestingly, BE mice showed the highest coherence value at alpha, beta, and low gamma frequencies ($p<0.01$), which is significantly different from the values observed in BACHD. Thus, the degree of synchronization between M1 and DS is highest in the conditional BE model followed by BACHD and WT mice.

We also evaluated relative phase between M1 and DS LFPs (Figure 6). BACHD mice showed a significant decrease in coherence phase in alpha ($p<0.0001$) and low gamma ($p<0.0001$) frequencies compared to WT (Figure 6A). Likewise, relative to WT, BE mice showed a significant decrease in alpha ($p<0.0001$) and low gamma ($p<0.0001$) bands. Between BE and BACHD, we observed an improvement in BE alpha ($p=0.001$) and gamma ($p<0.0001$) coherence phase. Analysis of the mean relative-phase value across the frequency spectrum indicated significant differences between groups ($p<0.0001$). LFPs in M1 and DS in WT mice show a phase lag of ~1.5°, indicating a lead role for M1. In contrast, M1 and DS LFP activity in BACHD was almost

perfectly in phase, showing a DS phase lead of ~ -0.5 ° (Figure 6B). Surprisingly, BE mice showed a phase lag of ~ -6°, indicating a DS lead.

Discussion

We found that BACHD mice progressively develop signs of behavioral inflexibility as exhibited by reduced turning during spontaneous exploration of the plus-shaped maze. This behavioral sign occurs along with alterations in corticostriatal LFPs. In contrast, the conditional BE model, which lacks *mHTT* expression in cortical output neurons, showed no aging-related change in plus-maze turning along with partial restoration of M1 LFP activity. Taken together, our results implicate M1 outputs in the development of motor inflexibility, a phenotype observed in both HD patients (Brouwers et al. 1984) and HD transgenic models (Hong et al. 2012b). Our results also add further support to evidence that cortical outputs play a key role in the motor processing deficits in HD (Estrada-Sánchez et al. 2015b).

Evidence obtained from HD patients also supports the contribution of cortical outputs to HD neuropathology. Patients with bradykinesia and dystonia as the main HD phenotype, for example, show enhanced thinning in premotor and supplementary motor areas relative to patients with other HD signs (Rosas et al. 2008; for review see Estrada-Sánchez and Rebec 2013b). Thus, neuropathology in the cerebral cortex is a likely contributor to the development of impaired neuronal communication in HD, which, as the disease progresses, will trigger phenotypical changes, including motor inflexibility. Interestingly, this motor phenotype in HD patients has been described in relation to cognitive and spatial perception tasks (Hanes et al. 1995; Brouwers et al. 1984), most likely due to an effect on multiple corticostriatal circuits.

Behavioral inflexibility refers to the inability to switch ongoing behavior in response to environmental demands (Ragozzino, 2007; Brown and Tait 2014). In HD, this can be manifest, in

293 part, as stereotyped behavior in which a particular set of motor commands are repetitively
294 executed. Stereotypic behaviors are observed in several neuropathological conditions related to
295 corticostriatal dysfunction, including HD (Crittenden et al. 2014; Zike et al. 2017; Cyr et al. 2006;
296 Chen et al. 2013). The plus-shaped maze provides a quantifiable measure of stereotypy as a
297 decreased propensity to turn into the left or right arm and instead to continue straight into the
298 opposite arm (Hong et al. 2012b). By studying LFP changes in the conditional BE model during
299 plus-maze turning, we can assess the role of M1 *mHTT* in the development of motor inflexibility
300 as HD progresses.

301 Because motor inflexibility in BACHD mice develops with aging, we evaluated M1 and
302 DS LFP changes in the oldest mice (50-64 weeks of age) as they entered and exited the choice
303 point. In M1, BACHD mice showed a significant decrease in alpha, beta, and low gamma power
304 that was at least partially reversed in BE mice. Although the combined dysregulation of these
305 frequency bands may contribute to the decrease in BACHD turning, a change in beta activity stands
306 out because of its link to motor control (Feingold et al. 2015). The precise role of these M1 rhythms
307 in behavior remains speculative, however, and their behavioral relevance should be evaluated in
308 follow-up work. In DS, surprisingly, the BE model failed to reverse the significant decrease in all
309 the frequency bands we evaluated, and even promoted a further decrease below BACHD power
310 for beta as well as theta and low gamma. These changes in DS activity may represent a
311 compensatory response to the suppression of mhtt in cortical outputs.

312 Although DS involvement in the improved behavioral responding in BE mice is unclear, it
313 is unlikely that the oscillations we recorded in DS can be explained by volume conduction from
314 M1 (see Lalla et al. 2017). The disparity between M1 and DS activity at all the frequency bands
315 we studied argues against this explanation. The disparity, however, is difficult to reconcile with a

direct monosynaptic connection between M1 and DS. In fact, a common view of corticostriatal connectivity is that cortex drives striatum to shape motor output. By integrating sensorimotor and reward information, cortex is thought to mediate situational responding, while striatum consolidates learned routines into habits (Graybiel, 2008; Howe et al. 2011). But striatum, which also integrates sensorimotor and reward information, can be just as critical in shaping behavior (Bar-Gad et al. 2003; Houk and Wise 1995). Striatum, for example, responds more rapidly than cortex during associative learning, and striatal responses emerge first as learning occurs (Pasupathy and Miller 2005). Thus, although the neural correlates of behavior have been observed in cortex and striatum, the underlying driver-receiver dynamics remain unclear. Equally important is our finding that corticostriatal communication can be bidirectional depending on behavioral state (Nakhnikian et al. 2014), indicating that effective connectivity between cortex and striatum is neither unidirectional nor static.

We cannot attribute a change in individual M1 frequency bands to a particular neuronal population since multiple cell types are likely to contribute, including pyramidal neurons and interneurons as well as inputs from other structures such as thalamus. Various research approaches, for example, have suggested that the delta oscillation, which consistently shows changes in HD, might originate from both thalamus and from an intrinsic cell population within cortex such as interneurons (Amzica et al. 1992; Carracedo et al. 2013; Hall et al. 2014). In fact, impaired interneuron function has been described in HD, and a computational model of neural activity in HD mice indicates a reorganization of cortico-striatal drive related to altered synaptic coupling mediated in part by interneuron activity (Naze et al. 2018). In BACHD mice, progressive changes in spontaneous inhibitory and excitatory postsynaptic currents parallel the worsening HD phenotype (Spampanato et al. 2008). Changes in the dopamine system also have been linked to

dysfunctional corticostriatal neuronal processing in HD and the development of motor inflexibility (Chen et al. 2013). Down-regulation of expression and functioning of dopamine receptors and transporters have been reported for both HD postmortem brains and transgenic models including the R6/1, R6/2, and YAC128 mouse and the BACHD rat model (for a review see Rangel-Barajas and Rebec, 2016). However, a possible up-regulation of dopamine activity early in HD, which may account for signs of chorea, complicate dopamine involvement.

The plus-maze is a hippocampal-dependent behavior in which navigation, coding the sequence of events, and spatial working memory are involved (McDonald and White, 1993). Although evidence indicates that impaired synaptic plasticity occurs in the hippocampus in HD mice (Murphy et al. 2000; Milnerwood et al. 2006; Kolodziejczyk et al. 2014), it is unknown if impaired hippocampal functioning might also contribute to decreased motor inflexibility in BACHD mice and whether the lack of expression of mutant huntingtin in the conditional BE model would improve either hippocampal activity and/or turning probability. Nonetheless, this is an interesting question that deserves to be evaluated.

Coherence analysis provides a measure of the degree of synchrony between M1 and DS across the power spectrum. Our results indicate that as frequency increases significant reductions in M1-DS synchrony occur in WT, BE, and BACHD mice. A similar result has been reported for the R6/2 mouse model (Hong et al. 2012b). Interestingly, however, the decline in synchrony in BE mice is not as steep as in WT and BACHD, indicating a stronger M1-DS coherence particularly at alpha, beta, and low gamma frequency bands. Coherence analysis that includes downstream structures in basal ganglia and parts of thalamus may shed additional light on the M1-DS interaction during HD.

Our coherence-phase analysis revealed a significant change in the alpha and low gamma bands. In the alpha band, BE mice were intermediate between WT and BACHD, but strongly negative in low gamma. Previous evaluations of LFP activity in HD models have shown lower absolute delta and theta power in cortex and striatum of freely behaving and anesthetized R6/2 mice (Miller et al. 2011; Callahan and Abercrombie 2015). Increased theta/alpha (4-12 Hz) power also has been described in the globus pallidus of a HD patient (Groiss et al. 2011). Studies evaluating brain activity through quantitative electroencephalography also have revealed changes in the lower frequency bands in zQ175 and R6/2 mice (Fisher et al. 2013; Kantor et al. 2013). Collectively, these results further support the claim that changes in lower frequency bands (theta and alpha) may serve as a putative biomarker for HD progression (Leuchter et al. 2017).

Analysis of the corticostriatal relative phase indicates phase leads and lags from M1 to DS. The mean relative phase for WT indicated a lead role for M1, while BACHD mice were almost perfectly in phase and BE mice showed a phase lag. These results contrast with R6/2 data in which cortical and striatal LFPs were almost perfectly in phase with only a slight cortical lead and WT mice had a strong striatal lead indicated by a phase lag of 15-20 degrees (Hong et al. 2012b). The R6/2 data, however, represent a different mouse strain than BACHD and were collected in an open-field arena rather than a plus-maze.

Overall, our results support the hypothesis that *mHTT* in cortical pyramidal neurons is a key component of the dysfunctional neural circuitry underlying the HD behavioral phenotype. Impaired functioning of these neurons contributes to the development of two main hallmarks of HD: impaired corticostriatal processing and motor inflexibility. Although striatum is often the target of therapeutic strategies for HD, our results continue to suggest a role for cortical mechanisms.

Acknowledgements: This work was supported by CHDI Foundation. We also acknowledge Dr. X. William Yang (UCLA) for providing the mice. We thank Paul Langley for technical support. AGH is supported by the National Institutes of Health, Ruth L. Krischtein National Research Service Award (T32 NS058280).

Conflict of Interest: The authors declare no competing financial interests.

References

Amzica F, Nuñez A, Steriade M. Delta frequency (1-4 Hz) oscillations of perigeniculate thalamic neurons and their modulation by light. *Neuroscience* 51: 285-294, 1992.

Bar-Gad I, Morris G, Bergman H. Information processing, dimensionality reduction and reinforcement learning in the basal ganglia. *Prog Neurobiol* 71: 439-473, 2003.

Brouwers P, Cox C, Martin A, Chase T, Fedio P. Differential perceptual-spatial impairment in Huntington's and Alzheimer's dementias. *Arch Neurol* 41: 1073-1076, 1984.

Brown VJ, Tait DS. Behavioral flexibility: attentional shifting, rule switching, and response reversal. In *encyclopedia of psychopharmacology*. Pp. 209-213. Editor: Stolerman IP. 2010. Springer-Verlag Berlin Heidelberg.

Callahan JW, Abercrombie ED. Relationship between subthalamic nucleus neuronal activity and electrocorticogram is altered in the R6/2 mouse model of Huntington's disease. *J Physiol* 593: 3727-3738, 2015.

Carracedo LM, Kjeldsen H, Cunnington L, Jenkins A, Schofield I, Cunningham MO, Davies CH, Traub RD, Whittington MA. A neocortical delta rhythm facilitates reciprocal interlaminar interactions via nested theta rhythms. *J Neurosci* 33: 10750-10761, 2013.

Chen JY, Wang EA, Cepeda C, Levine MS. Dopamine imbalance in Huntington's disease: a mechanism for the lack of behavioral flexibility. *Front Neurosci* 7:114, 2013.

Crittenden JR, Lacey CJ, Lee T, Bowden HA, Graybiel AM. Severe drug-induced repetitive behaviors and striatal overexpression of VAChT in ChAT-ChR2-EYFP BAC transgenic mice. *Front Neural Circuits* 8:57, 2014.

Cyr M, Sotnikova TD, Gainetdinov RR, Caron MG. Dopamine enhances motor and neuropathological consequences of polyglutamine expanded huntingtin. *FASEB J* 20: 2541–2543, 2006.

De la Monte SM, Vonsattel JP, Richardson EP Jr. Morphometric demonstration of atrophic changes in the cerebral cortex, white matter, and neostriatum in Huntington's disease. *J Neuropathol Exp Neurol* 1988 47: 516-525, 1988.

Estrada-Sánchez AM, Barton SJ, Rebec GV. Altered neuronal dynamics in the striatum on the behavior of huntingtin interacting protein 14 (HIP14) knockout mice. *Brain Sci* 3: 1588-1596, 2013a.

Estrada-Sánchez AM, Bunner KD, Rebec GV. Huntington's disease and dementia: from transgenic models to molecular neuropathology. In: *diet and nutrition in dementia and cognitive decline*, edited by Martin CR. Preddy VR: Cambridge, MA: Academic Press, 77–91. (2015a).

Estrada-Sánchez AM, Burroughs CL, Cavaliere S, Barton SJ, Chen S, Yang XW, Rebec GV. Cortical efferents lacking mutant huntingtin improve striatal neuronal activity and behavior in a conditional mouse model of Huntington's disease. *J Neurosci* 35: 4440-4451, 2015b.

Estrada-Sánchez AM, Rebec GV. Role of cerebral cortex in the neuropathology of Huntington's disease. *Front Neural Circuits* 7:19, 2013b.

Feingold J, Gibson DJ, DePasquale B, Graybiel AM. Bursts of beta oscillation differentiate post-performance activity in the striatum and motor cortex of monkeys performing movement tasks. *Proc Natl Acad Sci, USA* 112:13687-13692, 2015.

Fisher SP, Black SW, Schwartz MD, Wilk AJ, Chen TM, Lincoln WU, Liu HW, Kilduff TS, Morairty SR. Longitudinal analysis of the electroencephalogram and sleep phenotype in the R6/2 mouse model of Huntington's disease. *Brain* 136: 2159–2172, 2013.

Fowler SC, Miller BR, Gaither TW, Johnson MA, Rebec GV. Force-plate quantification of progressive behavioral deficits in the R6/2 mouse model of Huntington's disease. *Behav Brain Res* 202: 130-137, 2009.

Gray M, Shirasaki DI, Cepeda C, André VM, Wilburn B, Lu XH, Tao J, Yamazaki I, Li SH, Sun YE, Li XJ, Levine MS, Yang XW. Full-length human mutant huntingtin with a stable polyglutamine repeat can elicit progressive and selective neuropathogenesis in BACHD mice. *J Neurosci*. 28: 6182-6195, 2008.

Graybiel, AM. Habits, rituals, and the evaluative brain. *Annu Rev Neurosci* 31:359-387, 2008.

Groiss SJ, Elben S, Reck C, Voges J, Wojtecki L, Schnitzler A. Local field potential oscillations of the globus pallidus in Huntington's disease. *Mov Disord* 26: 2577-2578, 2011.

Gusella JF, Wexler NS, Conneally PM, Naylor SL, Anderson MA, Tanzi RE, Watkins PC, Ottina K, Wallace MR, Sakaguchi AY, Young AB, Shoulson I, Bonilla E, Martin. A polymorphic DNA marker genetically linked to Huntington's disease. *Nature* 306: 234-238, 1983.

Hall TM, de Carvalho F, Jackson A. A common structure underlies low-frequency cortical dynamics in movement, sleep, and sedation. *Neuron* 83: 1185-1199, 2014.

Halliday GM, McRitchie DA, Macdonald V, Double KL, Trent RJ, McCusker E. Regional specificity of brain atrophy in Huntington's disease. *Exp Neurol* 154: 663-672, 1998.

Hanes KR, Andrewes DG, Pantelis C. Cognitive flexibility and complex integration in Parkinson's disease, Huntington's disease, and schizophrenia. *J Int Neuropsychol Soc* 1: 545-553, 1995.

Hong SL, Barton SJ, Rebec GV. Altered neural and behavioral dynamics in Huntington's disease: an entropy conservation approach. *PLoS One* 7: e30879, 2012a.

Hong SL, Cossyleon D, Hussain WA, Walker LJ, Barton SJ, Rebec GV. Dysfunctional behavioral modulation of corticostriatal communication in the R6/2 mouse model of Huntington's disease. *PLoS One* 7:e47026, 2012b.

Houk JC, Wise SP. Distributed modular architectures linking basal ganglia, cerebellum, and cerebral cortex: their role in planning and controlling action. *Cereb Cortex* 5: 95-110, 1995.

Howe MW, Atallah HE, McCool A, Gibson DJ, Graybiel AM. Habit learning is associated with major shifts in frequencies of oscillatory activity and synchronized spike firing in striatum. *Proc Natl Acad Sci, USA* 108: 16801-16806, 2011.

Kantor S, Szabo L, Varga J, Cuesta M, Morton AJ. Progressive sleep and electroencephalogram changes in mice carrying the Huntington's disease mutation. *Brain* 136: 2147–2158, 2013.

Kim EH, Thu DC, Tippett LJ, Oorschot DE, Hogg VM, Roxburgh R, Synek BJ, Waldvogel HJ, Faull RL. Cortical interneuron loss and symptom heterogeneity in Huntington disease. *Ann Neurol* 75: 717-727, 2014.

Kolodziejczyk K, Parsons MP, Southwell AL, Hayden MR, Raymond LA. Striatal synaptic dysfunction and hippocampal plasticity deficits in the Hu97/18 mouse model of Huntington disease. *PLoS One* 9:e94562, 2014.

Lalla L, Rueda Orozco PE, Jurado-Parras MT, Brovelli A, Robbe D. Local or not local: investigating the nature of striatal theta oscillations in behaving rats. *eNeuro* 4 (5) e0128-17, 2017.

Leuchter MK, Donzis EJ, Cepeda C, Hunter AM, Estrada-Sánchez AM, Cook IA, Levine MS, Leuchter AF. Quantitative electroencephalographic (qEEG) biomarkers in preclinical and human studies of Huntington's disease: are they fit-for-purpose for treatment development? *Front Neurol* 8: 91, 2017.

McDonald RJ, White NM. A triple dissociation of memory systems: hippocampus, amygdala, and dorsal striatum. *Behav Neurosci* 107: 3, 1993.

Miller BR, Walker AG, Barton SJ, Rebec GV. Dysregulated neuronal activity patterns implicate corticostriatal circuit dysfunction in multiple rodent models of Huntington's disease. *Front Syst Neurosci* 5:26, 2011.

Milnerwood AJ, Cummings DM, Dallérac GM, Brown JY, Vatsavayai SC, Hirst MC, Rezaie P, Murphy KP. Early development of aberrant synaptic plasticity in a mouse model of Huntington's disease. *Hum Mol Genet* 15: 1690, 2006.

Murphy KP, Carter RJ, Lione LA, Mangiarini L, Mahal A, Bates GP, Dunnett SB, Morton AJ. Abnormal synaptic plasticity and impaired spatial cognition in mice transgenic for exon 1 of the human Huntington's disease mutation. *J Neurosci* 20: 5115, 2000.

Nakhnikian A, Rebec GV, Grasse LM, Dwiel LL, Shimono M, Beggs JM. Behavior modulates effective connectivity between cortex and striatum. *PLoS ONE* 9:e89443, 2014.

Naze S, Humble J, Zheng P, Barton S, Rangel-Barajas C, Rebec GV, Kozloski JR. Cortico-striatal cross-frequency coupling and gamma genesis disruptions in Huntington's disease mouse and computational models. *eNeuro* 5: e0210, 2018.

Pasupathy A, Miller EK. Different time courses of learning-related activity in the prefrontal cortex and striatum. *Nature* 433: 873-876, 2005.

Paxinos G, Franklin KBJ. The mouse brain in stereotaxic coordinates. Ed 2. San Diego: Academic; 2001.

Ragozzino ME. The contribution of the medial prefrontal cortex, orbitofrontal cortex, and dorsomedial striatum to behavioral flexibility. *Ann N Y Acad Sci* 1121: 355-375, 2007.

Rangel-Barajas C, Estrada-Sánchez AM, Barton SJ, Luedtke RR, Rebec GV. Dysregulated corticostriatal activity in open-field behavior and the head-twitch response induced by the hallucinogen 2,5-dimethoxy-4-iodoamphetamine. *Neuropharmacology* 113: 502-510, 2017.

Rangel-Barajas C, Rebec GV. Dysregulation of Corticostriatal Connectivity in Huntington's Disease: A Role for Dopamine Modulation. *J Huntingtons Dis* 5:303-331, 2016.

Rebec GV, Barton SJ, Marseilles AM, Collins K. Ascorbate treatment attenuates the Huntington behavioral phenotype in mice. *Neuroreport* 14: 1263-1265, 2003.

Rosas HD, Salat DH, Lee SY, Zaleta AK, Pappu V, Fischl B, Greve D, Hevelone N, Hersch SM. Cerebral cortex and the clinical expression of Huntington's disease: complexity and heterogeneity. *Brain* 131: 1057-1068, 2008.

Spampanato J, Gu X, Yang XW, Mody I. Progressive synaptic pathology of motor cortical neurons in a BAC transgenic mouse model of Huntington's disease. *Neuroscience* 157: 606-620, 2008.

The Huntington's Disease Collaborative Research Group. A novel gene containing a trinucleotide repeat that is expanded and unstable on Huntington's disease chromosomes. *Cell* 72: 971-983, 1993.

Thu DC, Oorschot DE, Tippett LJ, Nana AL, Hogg VM, Synek BJ, Luthi-Carter R, Waldvogel HJ, Faull RL. Cell loss in the motor and cingulate cortex correlates with symptomatology in Huntington's disease. *Brain* 133:1094-1110, 2010.

Zike ID, Chohan MO, Kopelman JM, Krasnow EN, Flicker D, Nautiyal KM, Bubser M, Kellendonk C, Jones CK, Stanwood G, Tanaka KF, Moore H, Ahmari SE, Veenstra-VanderWeele J. OCD candidate gene SLC1A1/EAAT3 impacts basal ganglia-mediated activity and stereotypic behavior. *Proc Natl Acad Sci, USA* 114: 5719-5724, 2017.

Wang N, Gray M, Lu XH, Cantle JP, Holley SM, Greiner E, Gu X, Shirasaki D, Cepeda C, Li Y, Dong HW, Levine MS, Yang XW. Neuronal targets of mutant huntingtin genetic reduction to ameliorate Huntington's disease pathogenesis in mice. *Nat Medi* 20: 536-541, 2014.

Figure legends

Figure 1. Age-related turning in the plus-shaped maze. WT, BE, and BACHD mice were allowed to explore the plus-shaped maze for 30 min and the probability of turning was calculated as the sum of arm choices (right or left arm) divided by the total number of arm choices. (A) Mixed-effects, two-way ANOVA with repeated measures shows a decline in turning probability in BACHD mice relative to WT ($p=0.0149$) and BE mice ($p=0.0343$; n=50 trials for WT; n=56 trials for BACHD; n=60 trials for BE). WT and BE mice show similar turning probability ($p=0.999$). (B) A similar number of total arm entries were observed across genotypes ($p>0.05$; n=50 trials for WT; n=56 trials for BACHD; n=60 trials for BE mice). Only data from 25 to 50 weeks of age were included due to some older mice losing their headstage. (C) Linear regression plot of the probability of turning assessed at regular intervals for mice that remained in the study up to 64 weeks of age. Although WT (n=6) and BE mice (n=6) showed an almost identical slight decline (non-significant difference from zero slope; ($p=0.363$, $r^2=0.013$, n=67 trials for WT; and $p=0.108$, $r^2=0.034$, n=73 trials for BE), BACHD mice (n=6) exhibited a reduction in turning probability as they aged (significant deviation from zero * $p=0.0006$; $r^2= 0.15$; n=76 trials). (D) Linear regression plot of the total number of arm entries during each recording session. All mice continued to explore the maze as they aged. The arm-entry slope is not significantly different from zero for all groups ($p=0.10$, $r^2=0.041$, n=67 for WT; $p=0.80$, $r^2=0.00085$, n=73 for BE; and $p=0.28$, $r^2=0.015$, n=76 for BACHD), indicating that all groups were comparably active. * indicates significant difference relative to WT ($p< 0.05$). ☆ indicates a significant difference relative to BE mice ($p< 0.05$).

Figure 2. Schematic representation of electrode placements corroborated by histological analysis. Shading indicates location of placements in M1 cortex and DS for WT, BE and BACHD mice as indicated at coronal section +0.5 mm anterior to bregma.

Figure 3. Cortical LFPs. Mean (±SEM) band power (%PSD) of delta (A) theta (B), alpha (C), beta (D) and low gamma (E) in M1 cortex. Data for this and subsequent figures were obtained from mice 50 to 64 weeks of age. * indicates significant difference relative to WT. ☆ indicates significant difference relative to BE. Data were analyzed by means of a two-way ANOVA followed by Tukey's multiple comparison test. WT n = 581; BE = 848; BACHD = 446 events.

Figure 4. Striatal LFPs. Mean (±SEM) band power (%PSD) of delta (A) theta (B), alpha (C), beta (D) and low gamma (E) in DS. * indicates significant difference relative to WT. ☆ indicates significant difference relative to BE mice. Data were analyzed by means of a two-way ANOVA followed by Tukey's multiple comparison test. WT n = 581; BE = 848; BACHD = 446 events.

Figure 5. Coherence value of LFP activity between M1 and DS. Changes in the mean (±SEM) value of each indicated frequency band. Note an overall decline in coherence between M1 and DS as frequency increases. * indicates significant difference relative to WT ($p < 0.05$). ☆ indicates significant difference relative to BE mice ($p < 0.05$). Data were analyzed by means of a two-way ANOVA followed by Tukey's multiple comparison test. WT n = 581; BE = 848; BACHD = 446 events.

Figure 6. Mean phase relationships between M1 and DS. (A) Mean (±SEM) coherence phase across frequencies. (B) Relative phase values obtained from (A). * indicates significant difference relative to WT ($p < 0.05$). ☆ indicates significant difference relative to BE mice ($p < 0.05$). Data were analyzed by means of a two-way ANOVA followed by Tukey's multiple comparison test. WT = 581 events; BE = 848 events; BACHD = 446 events.

Figure 1

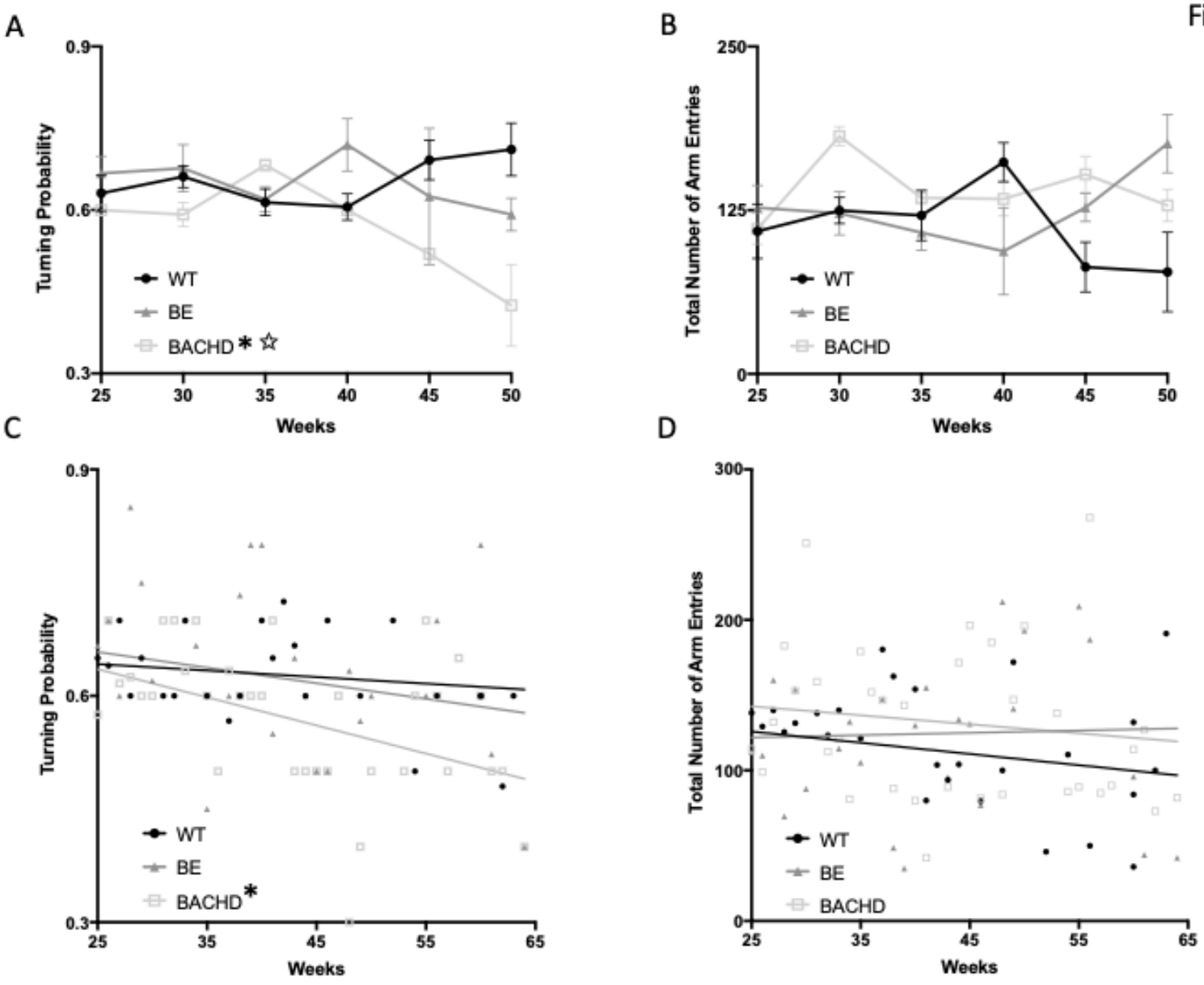

Figure 2

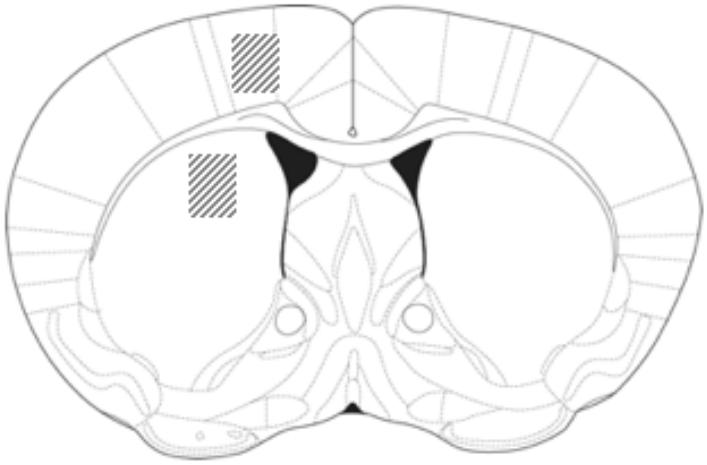

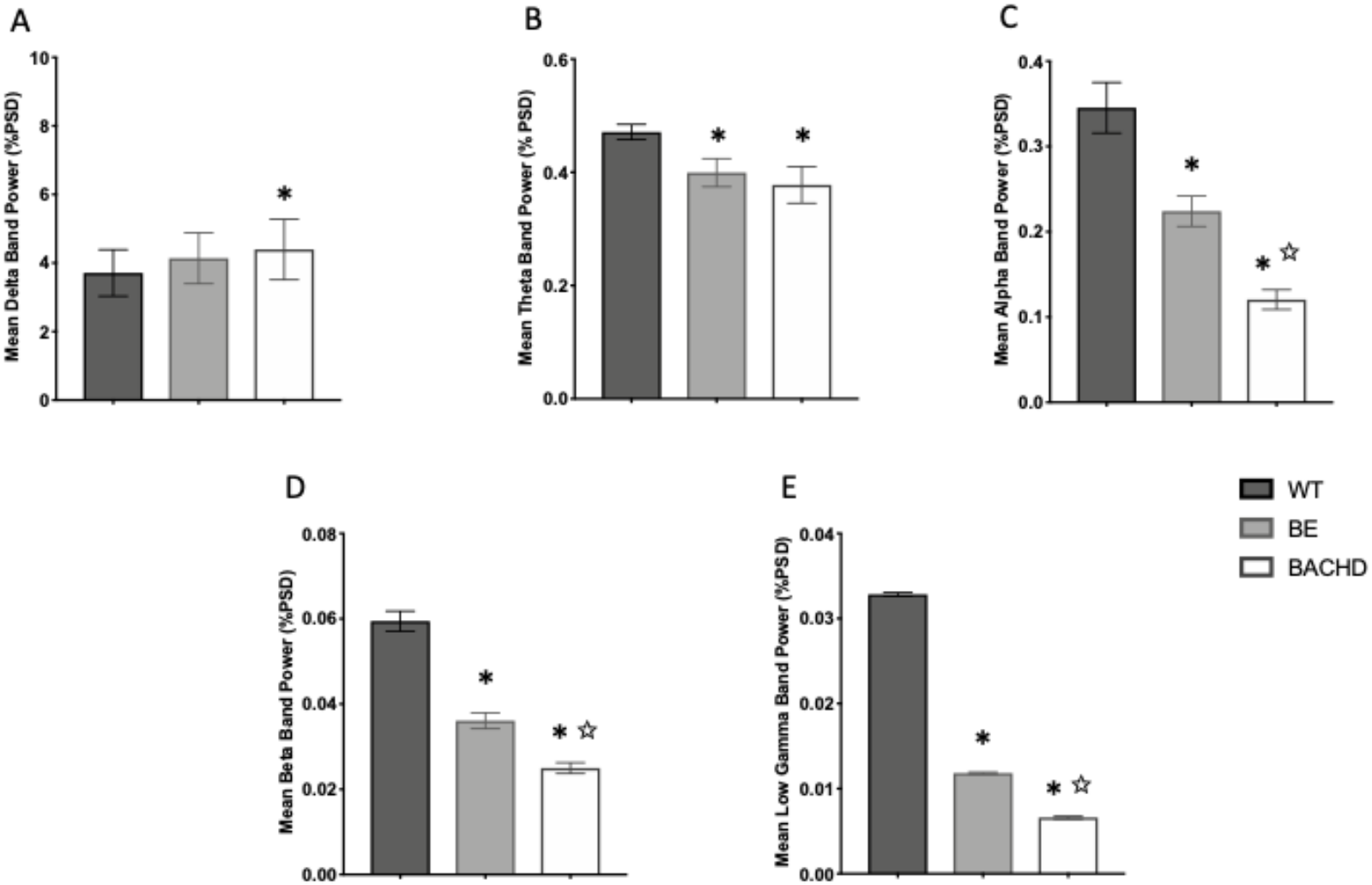

Figure 3

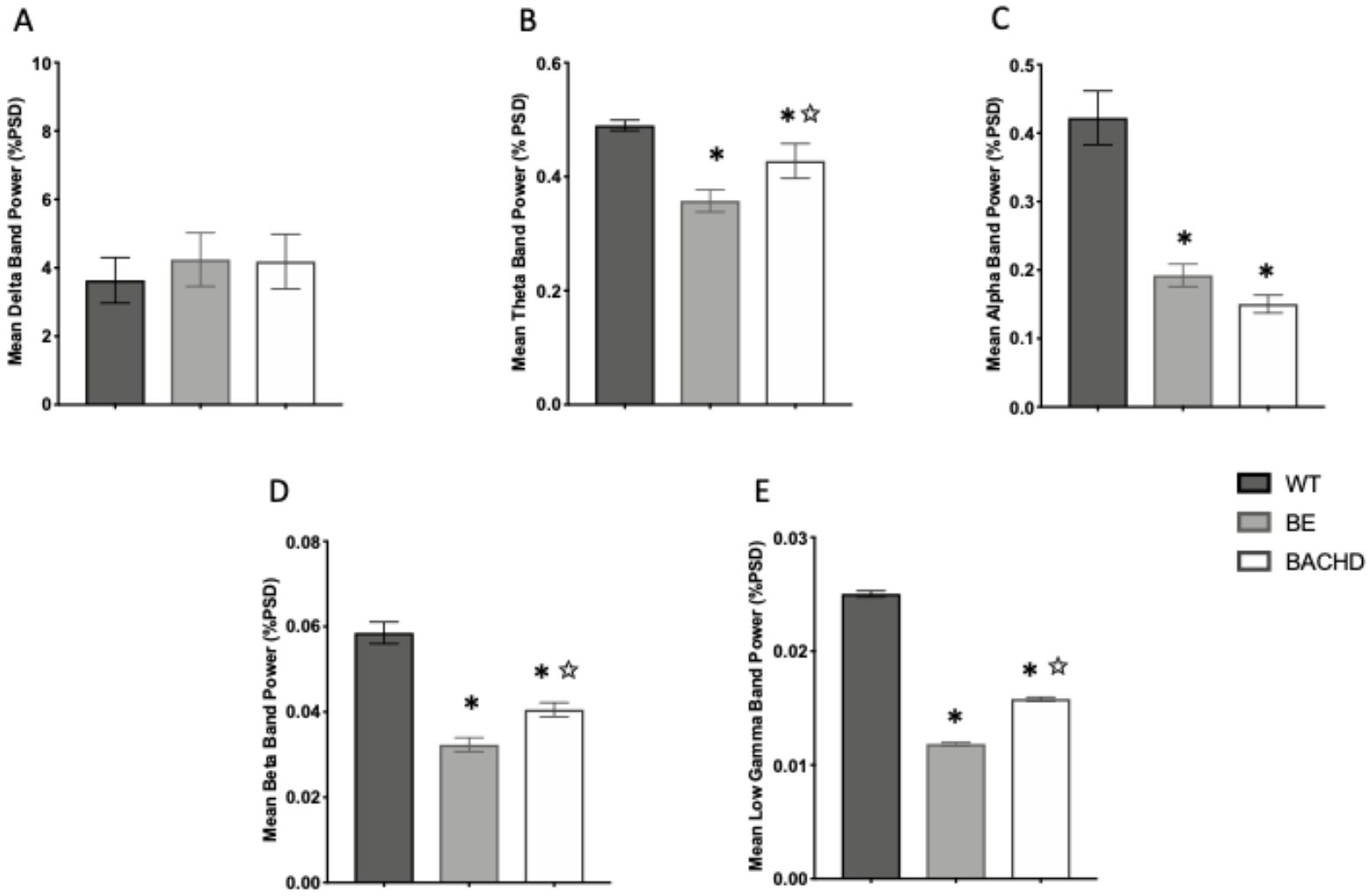

Figure 4

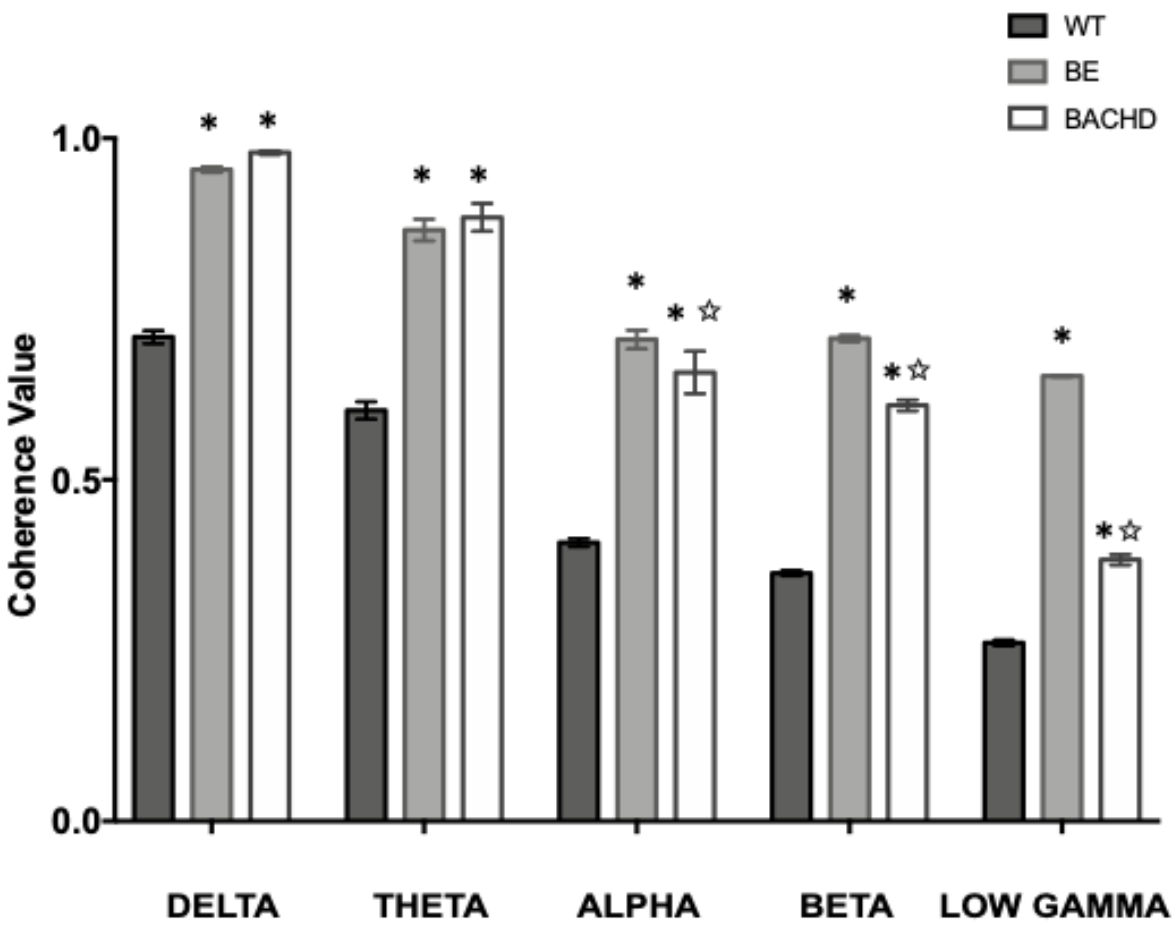

Figure 5

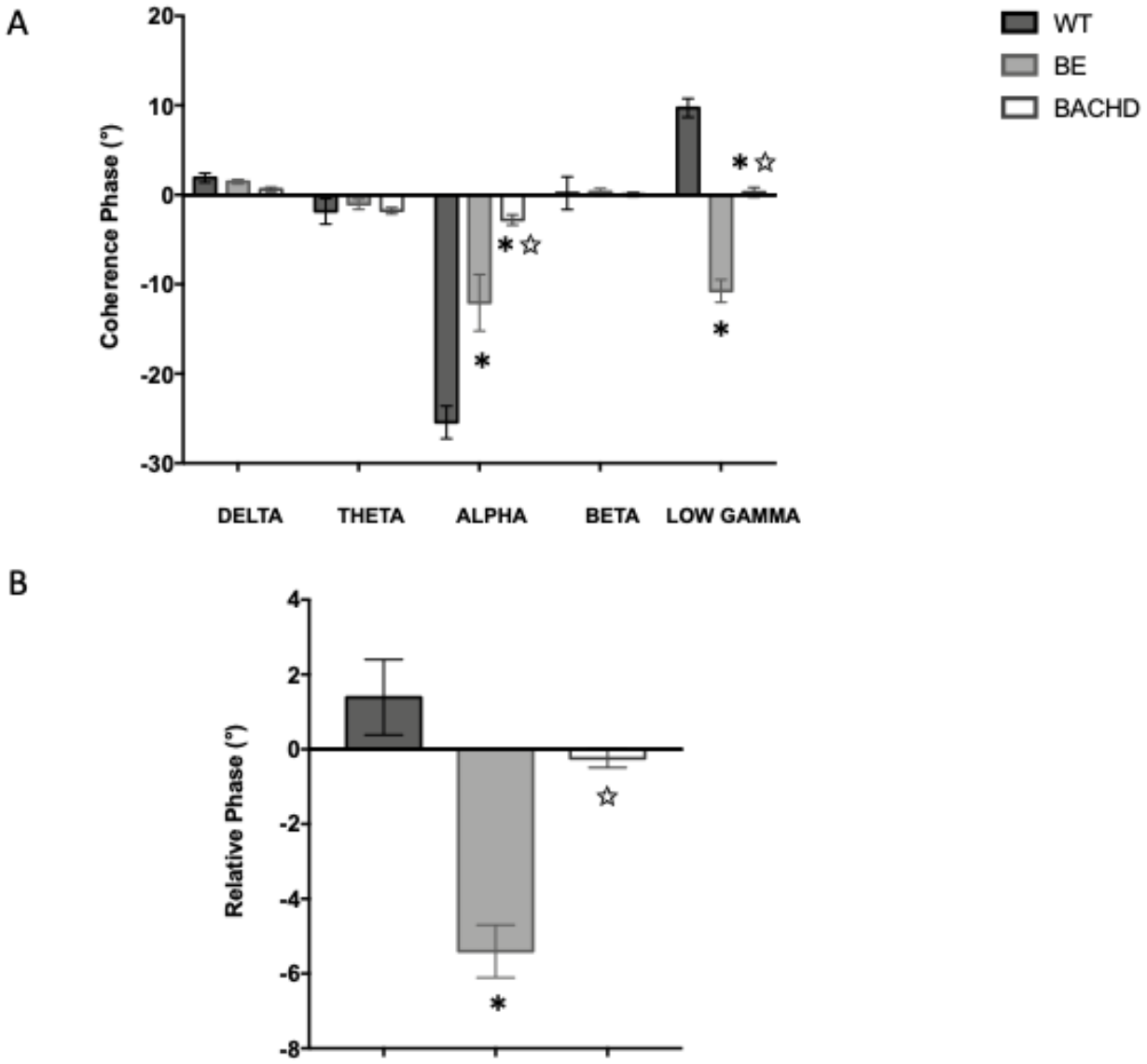

Figure 6